ChemPubSoc Europe

DOI: 10.1002/cssc.201500107

CHEMSUSCHEM Full Papers

Carbon-Nanotubes-Supported Pd Nanoparticles for Alcohol Oxidations in Fuel Cells: Effect of Number of Nanotube Walls on Activity

Jin Zhang,[a] Shanfu Lu,[b] Yan Xiang,[b] Pei Kang Shen,[c] Jian Liu,[a] and San Ping Jiang*[a]

Carbon nanotubes (CNTs) are well known electrocatalyst supports due to their high electrical conductivity, structural stability, and high surface area. Here, we demonstrate that the number of inner tubes or walls of CNTs also have a significant promotion effect on the activity of supported Pd nanoparticles (NPs) for alcohol oxidation reactions of direct alcohol fuel cells (DAFCs). Pd NPs with similar particle size (2.1–2.8 nm) were uniformly assembled on CNTs with different number of walls. The results indicate that Pd NPs supported on triple-walled CNTs (TWNTs) have the highest mass activity and stability for methanol, ethanol, and ethylene glycol oxidation reactions, as compared to Pd NPs supported on single-walled and multi-walled CNTs. Such a specific promotion effect of TWNTs on the electrocatalytic activity of Pd NPs is not related to the contribution of metal impurities in CNTs, oxygen-functional groups of CNTs or surface area of CNTs and Pd NPs. A facile charge transfer mechanism *via* electron tunneling between the outer wall and inner tubes of CNTs under electrochemical driving force is proposed for the significant promotion effect of TWNTs for the alcohol oxidation reactions in alkaline solutions.

Introduction

■■Change to title OK? Our guideline is approx. 120 characters including spaces. Please supply academic titles of authors ■■Direct alcohols fuel cells (DAFCs) have attracted considerable attention due to its high volumetric energy density of alcohols and ease of storage and transport of liquid fuels in comparison with hydrogen.[1,2] Pd nanoparticles (NPs) are the most common electrocatalysts in DAFCs because of their high activity for alcohol oxidation reactions in alkaline solutions.[3–7] However, Pd is a precious noble metal whose high cost impedes the commercialization of DAFCs. Thus, increasing the Pd activity for alcohols oxidation and decreasing the Pd loading in the catalyst layer are important for the DAFCs development.[8] High activity of Pd NPs is believed to result from high reaction surface area in terms of shape, size, and dispersion.[9] Thus, carbon materials have been extensively investigated as electrocatalyst supports in DAFCs to uniformly disperse metal nanoparticles and subsequently increase its electrocatalytic activity.[10] Compared with active carbon (Vulcan XC-72) and carbon fiber (CF), Pd NPs supported on multi-walled carbon nanotubes (MWNTs) demonstrated higher ethanol electrochemical oxidation activity in alkaline media owing to high surface area as well as the high electrical conductivity of CNTs.[11] The superior activity of Pd NPs supported on MWNT in comparison to those supported on high surface area carbons was also confirmed by Singh et al. in terms of the methanol oxidation reaction (MOR) and ethanol oxidation reaction (EOR).[12]

In general, the catalytic activity of metal catalysts for the alcohols oxidation reaction strongly depends on the nature of CNTs support in terms of the surface area, conductivity, and chemical properties.[13] Carmo et al.[14] investigated the catalytic activity of PtRu supported on single-walled carbon nanotubes (SWNT) and MWNT and found out that PtRu/SWNT showed higher MOR activity than PtRu/MWNT. Moreover, Pt NPs supported on CNTs also showed the same trend for MOR in acid solution; that is, the activity of Pt NPs on SWNTs was 34.3% higher than that of Pt-MWNTs.[15] The better activity of Pd NPs supported on SWNTs was attributed to the higher surface area of SWNTs. Besides high surface area, electronic conductivity of the carbon supports also affect the activity of metal NPs/CNTs.[16] Lukehart et al.[17] demonstrated that the relative activity of PtRu/carbon for MOR depends strongly on the electron transport rate along the axis of the carbon substrate to the current collection electrodes. In their study, DMFC performance of PtRu catalyst decreased in the order of carbon support: graphitic carbon nanofiber (GCNF) > SWNTs > MWNTs. The excellent catalytic performance of GCNF-supported PtRu is due to their high electronic conductivity, as electrons produced on the surface of GCNF could flow across the graphene sheet of the herringbone layers to the highly conducting tubular graphitic core. SWNTs show higher electronic conductivity than that of MWNTs because of the high crystalline graphitic structure of SWNT, consistent with the results of redox probe test.[18] Finally,

[a] J. Zhang, J. Liu, S. P. Jiang
Fuels and Energy Technology Institute
& Department of Chemical Engineering
Curtin University
Perth, WA 6102 (Australia)
E-mail: s.jiang@curtin.edu.au

[b] S. Lu, Y. Xiang
School of Chemistry and EnvironmentBeihang University
Beijing 100191 (China)

[c] P. K. Shen
Collaboarative Innovation Center of Sustainable Energy Materials
Guangxi University
Nanning 530004 (China)

the support materials could modify the catalyst in terms of the electron state of catalyst and the shape of the catalyst (geometric effect) as the metal catalysts are bonded on the surface of catalyst support. Yan et al speculated that the high MOR activity of PtRu supported on double-walled CNTs (PtRu/DWNTs) as compared to that of PtRu/MWNTs is due to the unique interaction between Pt and the DWNTs that facilitates charge transfer from Pt to the tubes, although the reasons were not explained.[19]

Most recently, we reported the electrocatalytic activity of Pd NPs supported on CNTs ranging from SWNTs, triple-walled CNT (TWNTs), to typical MWNTs for EOR in alkaline solutions.[20] The preliminary results indicate Pd NPs supported on CNTs with 3–7 walls show a higher EOR activity as compared with Pd NPs supported on SWNTs and MWNTs. Here we demonstrate for the first time that in addition to the EOR, Pd NPs supported on CNTs with 3–7 walls also have superior electrocatalytic activity for the electrochemical oxidation reaction of other popular alcohols, such as methanol, the simplest alcohol, and ethylene glycol (EG), the typical polyalcohol. EG has the relatively low toxicity, high boiling point, high specific energy (5.9 kWh L^{-1}) and is inexpensive and widely available as an interesting fuel in DAFCs. The electrocatalytic activity of Pd NPs supported on CNTs shows a distinctive volcano-type dependence on the number of walls of CNT supports for the oxidation of alcohols, clearly indicating that the promotion effect of the inner tubes ■■promotion effect of walls or of tubes?■■of CNT supports with 3–7 walls is a general phenomenon.

Results and Discussion

Characterizations of CNTs

The received CNTs samples contain trace of impurities resulting from the catalytic CVD ■■Please define■■synthesis of CNTs. Thus, the CNTs were treated by concentrated HCl solution to remove the impurities for the sake of eliminating the effect of impurities. After sonication of CNTs by concentrated HCl solution, the amount of Fe, Co, Mo, and Ni elements were substantially reduced ($<\sim$100 ppm) as confirmed by the ICP-OES analysis (Table S1, Supporting Information). The CNTs was then further examined by TEM in terms of morphology, wall number as well as outer diameter distribution (see Figure S1, Supporting Information). ■■Please add explanation of sample labelling. E.g. What is different in preparation of CNTs-1 and CNTs-2■■The number of walls and outer diameter of CNTs were taken as average over more than 10 TEM images for each CNTs sample. CNTs-1 consists of 79% SWNTs with outer diameter of 1.97 nm. CNTs-2 is dominated by triple-walled CNTs (52% TWNTs) with outer diameter of 3.80 nm. The average number of walls of CNTs-3 is seven with outer diameter of 7.45 nm, while CNTs-4 is typical MWNTs with average number of 12 walls and outer diameter of 13.90 nm. The average number of walls and size of the CNTs samples used in this study is given in Table 1. CNTs with small outer diameter prefers to form bundles consisting of two or more parallel tubes (marked by the white circles, Figure S1 A and B, Supporting Information) because of the van der Waals interactions;[21] however, CNTs with large outer diameters, CNTs-3 and CNTs-4, are dispersed without bundles.

Table 1. Average ourter diameter (OD), average wall numbers (n), I_D/I_G and BET surface area (S_{BET}), total volume (V_{total}), electrochemical accessible surface area (S_{CNTs}) and ratio of S_{CNTs}/S_{BET} of CNTs.

Sample	OD/nm	n	I_D/I_G	S_{BET} [$m^2 g^{-1}$]	V_{total} [$cm^{-3} g^{-1}$]	S_{CNTs} [$m^2 g^{-1}$]	S_{CNTs}/S_{BET} [%]
CNTs-1	1.97	1	0.16	577	1.06	126.7	22.0
CNTs-2	3.80	3	0.76	523	0.80	210.6	40.3
CNTs-3	6.90	7	1.35	539	0.81	190.5	35.4
CNTs-4	13.8	12	2.50	271	0.48	63.4	23.4

CNTs were examined by Raman spectroscopy at room temperature with excited laser wavelength and power density of 1064 nm^{-1} and 5 mW cm^{-2}, respectively (Figure 1 A). The D band in 1281 cm^{-1} derives from the amorphous carbon and defects, while the G band in 1589 cm^{-1} indicates the graphite layer of CNTs.[22] The intensity ratio of defect-derived D band (I_D) to graphite-derived G band (I_G) reflects destructiveness of the SP^2 hybridized carbon atom.[23,24] Thus, the increase of the I_D/I_G ratio is an indication of the destructiveness or the defect formation of the CNTs surface. I_D/I_G ratio is 0.16 for CNTs-1, consistent with SWNTs reported by Resasco.[25] In addition to the very small I_D/I_G ratio of 0.16, the presence of radial breathing modes (RBMs) confirms the SWNT structure in CNTs-1.[26] For CNTs-2, the ratio of RBMs intensity to D band intensity is higher than CNTs-1, suggesting the reduction of SWNTs proportion in CNTs-2 and increased multi-walled CNTs content. The ratio of I_D/I_G increases with the increase of the wall numbers of CNTs and when the wall number increase to 12 in CNTs-4, the I_D/I_G ratio is 2.5. Meanwhile, the absence of RBMs and the red-shift of D band in CNTs-4 shows that CNTs-4 contains ■■OK?■■typical MWNTs. This indicates the lower crystallinity of CNTs-4 than CNTs-1, CNTs-2 and CNTs-3, and consequently higher quantity of structural defects due to its multiple graphite layers.[27,28]

The tubular structure of CNTs was also characterized by N_2 adsorption–desorption isotherms, and specific surface areas as well as the pore size of CNTs were calculated accordingly (Figure 1 B). All CNTs samples showed the type IV isotherm with H3 hysteresis, indicating the mesoporous structure of CNTs. The sharp increase of nitrogen adsorption in the relative pressure region of 0.9–1.0 for CNTs-1 is attributed to the inner cavity among SWNT bundles, and this is supported by the pore size distribution of CNTs-1 with large pores of over 40 nm. Besides, the nitrogen adsorption at relative pressure under 0.1 in CNT-1 indicates the microporous feature of the SWNTs.[29] The Brunauer–Emmett–Teller (BET) surface area of CNTs-1, CNTs-2, CNTs-3, and CNTs-4 is 577 $m^2 g^{-1}$, 523 $m^2 g^{-1}$, 539 $m^2 g^{-1}$, and 271 $m^2 g^{-1}$, respectively (Table 1). The bundle structure of CNTs-1 and CNTs-2 decrease the surface area of

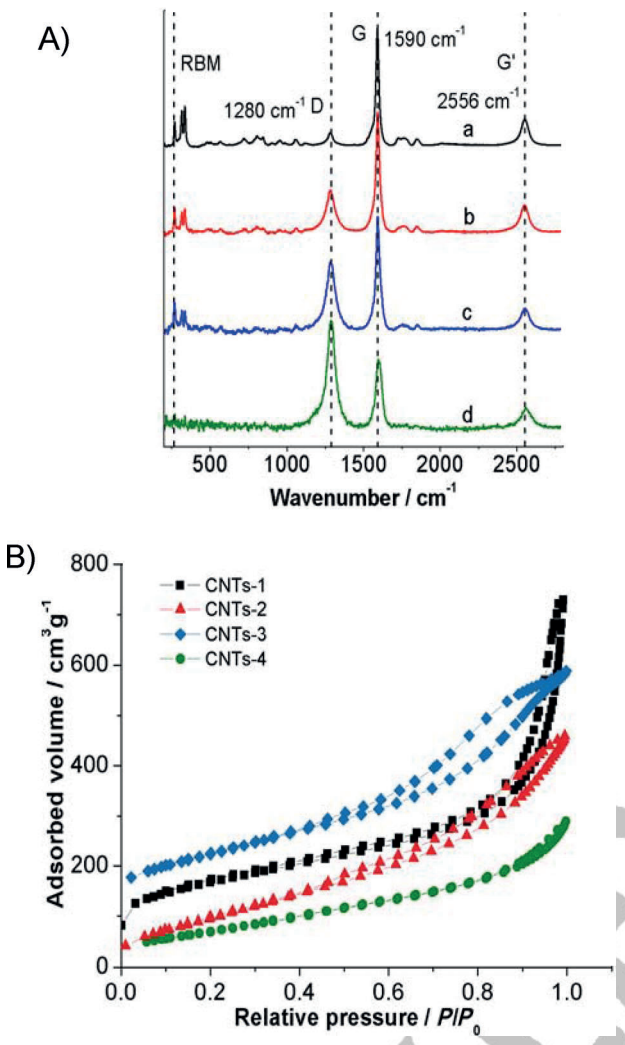

Figure 1. (A) Raman spectra of (a) CNTs-1, (b) CNTs-2, (d) CNTs-3 and (d) CNTs-4, and (B) the N_2 adsorption-desorption isotherms of CNTs.

CNTs-1 and CNTs-2,[30] while the sharply decrease of BET surface areas of CNTs-4 is most likely due to the increased diameter of MWNTs. The existence of pores with diameter of 3 nm indicates that the diameter of the inner tube is similar and the increase of number of walls increases the outer diameter of the CNTs.

Characterization of Pd-CNTs catalysts

Pd NPs were synthesized on CNTs surface via a self-assembly route with the assistance of tetrahydrofuran (THF) functionalization agent and were characterized by TEM (see Figure 2). Pd NPs with diameter of 2.1 to 2.8 nm are homogeneously dispersed on the surface of CNTs with no agglomeration, and the size is much smaller than 4.3–8.4 nm of Pd NPs on CNTs as reported in the literature.[8,12,31] The result indicates that THF is an effective agent to disperse the Pd NPs on the surface of CNTs (Figure 2A). The crystalline nature of Pd NPs was confirmed by XRD (Figure S3, Supporting Information). The peak at 25.9° is attributed to the hexagonal carbon structure of CNTs in (002) plane.[32] The 2θ values of 40.0° correspond to the diffraction peaks of Pd (111) with d-spacing of 0.23 nm, while 2θ value of 46.3°, 67.8°, and 80.6° correspond to Pd (200), Pd (220), and Pd (311), respectively. This confirms the face centered cubic (*fcc*) crystal structure of Pd NPs,[33] and the mean crystalline size was estimated to be 3.5 nm by Scherrer equation through the Pd(111) peak. In addition, the Pd (311) diffraction peak for Pd-CNTs-1 and Pd-CNTs-2 is discernible but of much low intensity, which may be due to the fact that Pd particles are small and high index facets are too weak to be clearly recognized.[34] Besides, according to the Rietveld analysis in the XRD pattern, there is no preferred orientation effect on Pd NPs.

XPS measurement was used to detect the surface state of CNTs and Pd NPs. No metal element impurities were detected in the XPS survey scan (Figure 3A), indicating that the acid purification successfully removed the majority of residual impurities of CNTs. The absence of Cl atoms also demonstrates that all the $[PdCl_4]^{2-}$ ions were reduced to Pd atoms by the H_2 reduction. Figure 3B shows the XPS spectra of C1s for the CNTs samples. Three peaks at 284.8 eV, 285.2 eV, and 286.4 eV associate with carbon atoms in graphite-like walls, carbon defects that are attributed to C atoms no longer in the regular tubular structure,[35] and high valence states C–O, respectively. Besides, the peak of 288.3 eV (–O–C=O), 289.0 eV (carbonates) presented in plasma treated CNTs are not detected in the CNTs samples,[35,36] indicating the relatively high degree of structural integrity of CNTs. By the curve fitting, the percentage of oxygen-containing surface functional groups is 1.5%, 8.2%, 6.7%, and 6.2% for CNTs-1, CNTs-2, CNTs-3 and CNTs-4, respectively. Except for CNTs-1, there is no substantial difference in oxygen-containing groups on CNTs-2 to CNTs-4.

The Pd3d signals in the XPS spectra of Pd-CNTs consist of two pairs of doublets for $Pd3d_{3/2}$ and $Pd3d_{5/2}$ (Figure 3C). In comparison with the standard spectra of metal Pd^0, the binding energy of $3d_{3/2}=341.1$ eV and $3d_{5/2}=335.8$ eV in Pd-CNTs are almost the same. Moreover, the high resolution Pd3d XPS reveals the positive shifts in the metallic Pd^0 peaks toward higher binding energy at 335.8 eV and 337.4 eV is assigned to the Pd^{II} state in PdO or $Pd(OH)_2$. The binding energy and element distribution are given in Table 2. The proportion of oxidized Pd increases from 44.3% to 67.3% as the number of CNT wall numbers increases from 1 to 12, respectively.

Table 2. XPS element state analysis and binding energy of $Pd3d_{5/2}$ of Pd-CNTs.

Sample	O/C	C–C [%]	C–O [%]	Ratio [%]		Binding energy of $Pd3d_{5/2}$ [eV]	
				Pd^0	Pd^{II}	Pd^0	Pd^{II}
Pd-CNTs-1	4.5	70.7	1.5	55.7	44.3	335.8	337.4
Pd-CNTs-2	4.9	68.2	8.2	40.7	59.3	335.8	337.4
Pd-CNTs-3	4.4	66.7	6.7	35.2	64.8	335.8	337.2
Pd-CNTs-4	4.2	72.6	6.2	32.7	67.3	335.8	336.9

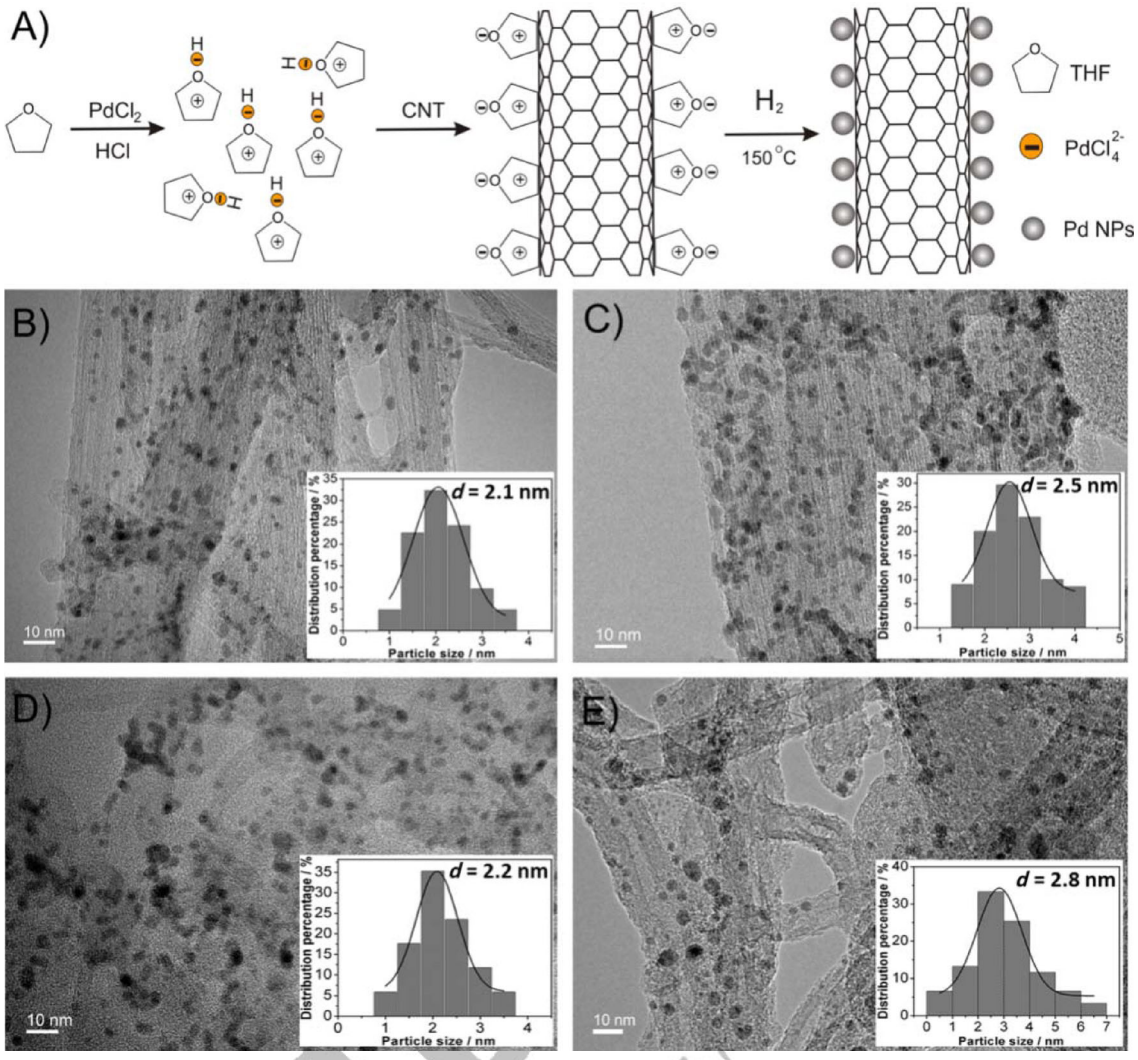

Figure 2. (A) Scheme of Pd-CNTs synthesis and TEM images of (B) Pd-CNTs-1, (C) Pd-CNTs-2, (D) Pd-CNTs-3, and (E) Pd-CNTs-4. Inset is histogram for Pd NPs of the catalysts.

Electrochemical activity of Pd-CNTs for alcohol oxidation reactions

The CO-stripping method was employed to measure the electrochemical active surface area (EASA) of Pd NPs, instead of the hydrogen-region integrated method, because Pd NPs have poor definition of hydrogen region due the adsorption of hydrogen to form Pd/H alloy.[37] A monolayer of CO was adsorbed on the surface of Pd NPs and then it was oxidized to CO_2 at ~0.8 V (*vs* RHE), as shown in Figure 4B. EASA values of Pd NPs were calculated from the CO oxidation peak areas. EASA of Pd-CNTs-2 is 36 $m^2 g^{-1}$, slightly higher than Pd-CNTs-1 (30 $m^2 g^{-1}$), while Pd-CNTs-3 has the highest value of 45 $m^2 g^{-1}$ among the four Pd-CNTs samples. In the case of CV measured in N_2-saturated 1.0 M KOH solution (Figure 4A), the results indicate that Pd-CNTs-3 has superior ability to adsorb OH^- ions in the alkaline solution. There is a broad oxidation peak around 0.4–0.6 V (vs RHE) in the forward scan (Figure 4A) and a similar peak was also observed on Pd black measured in N_2-saturated 1.0 M KOH solution (Figure S4, Supporting Information). The peak around 0.4–0.60 V in forward scan is most likely associated with OH^- adsorption. Similar broad peaks were also observed by Simoes et al on Pd/C in N_2-saturated 1.0 M NaOH solution.[38] Jeong et al studied the oxidation behavior of PdO in alkaline solution, using Pd disk electrode and identified formation of PdO_x ($x > 1$) at potential over 0.60 V (*vs* RHE).[39] Thus the broad oxidation peaks at 0.4–0.6 V in the forward scan is most likely associated with the incorporation of adsorbed OH^- ions and subsequent formation of PdO/PdO_x. In the backward scan, the PdO_x is reduced to Pd at 0.7 V to release the active site of Pd NPs. The OH^- adsorption peak density is in the order of Pd-CNTs-4 < Pd-CNTs-1 < Pd-CNTs-2 < Pd-CNTs-3.

Figure 5 shows the CV curves of CNTs in 1.0 M KOH with and without ethanol at a scan rate of 100 mV s^{-1}. The CV curve of CNTs-1 in the solution of 1.0 M KOH + 1.0 M ethanol almost overlapped with that measured in 1.0 M KOH, showing no oxidation current for the ethanol oxidation reaction. This indicates that pristine CNTs-1 has no electrocatalytic activity for EOR in alkaline solution. Other CNTs also demonstrate the same trend as CNTs-1. Despite the high BET surface area of CNTs-1, the

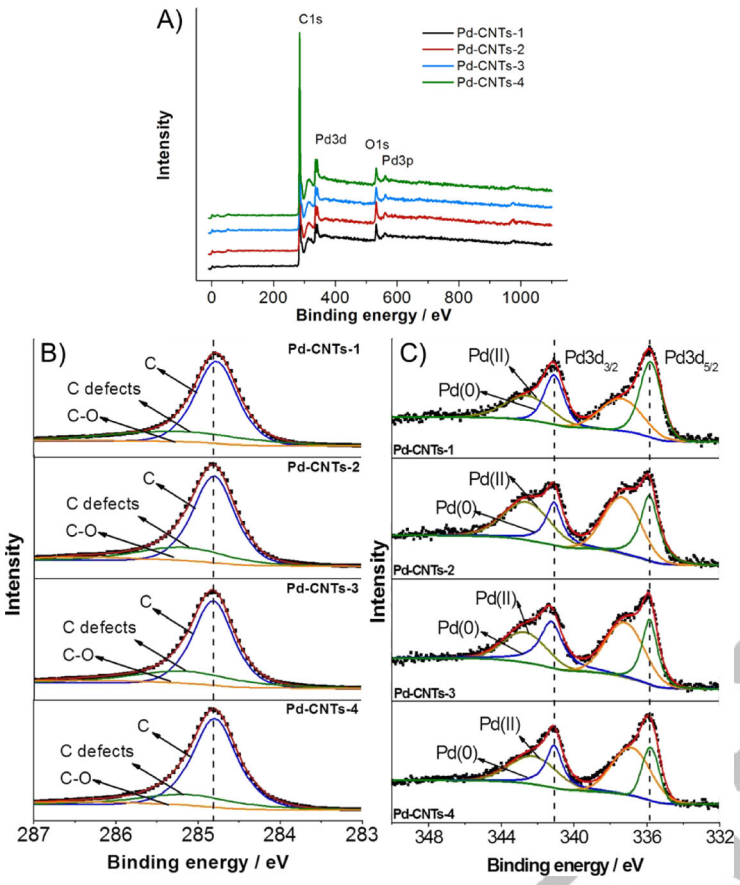

Figure 3. (A) Pd-CNTs XPS profile, (B) C1s core level XPS and (C) Pd 3d core level XPS.

double layer current of CNTs-1 is not the highest. The BET surface area of CNTs decreases with the increase of the wall number of CNTs, while the surface defects show the reverse trend against the wall number of CNTs.■■Please clarify sentence. The surface defects increase with wall number?■■ Thus, the low double layer current of CNTs-1 and CNTs-4 may be due to the trade-off between BET surface area and defects of CNTs. Also, there is no visible peak around 0.6 V (vs RHE) in the forward scans of the CV curves on pristine CNTs, confirming that the oxidation peak observed at 0.6 V in the case of Pd-CNTs (see Figure 4A) is not related to the impurities in CNTs.

Figure 6 shows that the CV curves of Pd-CNTs for the electrooxidation of methanol, ethanol and EG in alkaline solutions. Electrooxidation of methanol, ethanol, and ethylene glycol is characterized by well-separated anodic peaks in forward and reversed scans, consistent with that reported in the literatures.[40,41] The magnitude of the anodic current density in the forward scan is directly related to the amount of alcohols oxidized at Pd NPs. The electrocatalytic activity of Pd-CNTs strongly depends on the characteristics of CNT supports and the best results were observed on Pd NPs supported on CNTs-2 and CNTs-3. For the MOR of Pd-CNTs, the peak current density is 818 mA mg^{-1} and 780 mA mg^{-1} for Pd-CNTs-2 and Pd-CNTs-3, respectively, significantly higher than that of Pd-CNTs-1 (317 mA mg^{-1}) and Pd-CNTs-4 (501 mA mg^{-1}) (Figure 6A). The onset potential for Pd-CNTs-2 and Pd-CNTs-3 is 0.457 V and 0.478 V, which is also substantially more negative than 0.513 V observed on Pd-CNT-1 and 0.490 V on Pd-CNTs-4. The results indicate the significantly enhanced kinetics for the MOR on Pd-CNTs-2 and Pd-CNTs-3, showing the characteristic volcano curve of forward peak current density and U-shaped dependence of the onset potential for MOR as a function of number of walls of CNTs (Figure 6B).

Similarly, Pd NPs supported on CNTs-2 and CNTs-3 shows the highest electrochemical activities of 2858 mA mg^{-1} and 2469 mA mg^{-1} towards EOR, respectively, as compared to 1484 mA cm^{-2} and 1574 mA cm^{-2} for Pd-CNTs-1 and Pd-CNTs-4, respectively (Figure 6C). The onset potential is 0.353 V and 0.383 V for Pd-CNTs-2 and Pd-CNTs-3, respectively, which is lower than that on Pd-CNTs-1 and Pd-CNTs-4 (Figure 6D). In the case of EG oxidation reaction (EGOR), Pd-CNTs-2 and Pd-CNTs-3 have a superior electrochemical activity in terms of peak current density and onset potential (Figure 6E). The forward peak current density for EGOR is 2095 mA mg^{-1} on Pd-CNTs-2, 1.4–1.6 times of that measured on Pd-CNTs-1 and Pd-CNTs-4. The volcano curve of forward peak current density and U-shaped dependence of the onset potential for EGOR as a function of number of walls of CNTs (Figure 6F) are almost identical to that observed on MOR and EOR. The Pd-CNTs also show a much higher forward peak current density and lower onset potentials for MOR, EOR and EGOR, as compared to Pd NPs supported on high surface area carbon (XC-72),[42–44] consistent with the observations that CNT supports generally enhance the electrocatalytic activity of Pt and Pd NPs.[45] The electrocatalytic activity data of Pd-CNTs and Pd/C as reported in the literature are summarized in Table 3.

The electrochemical stability of Pd-CNTs during the alcohol oxidation was also investigated (Figure 7). The initial rapid decay in the current density for the methanol, ethanol, and EG oxidation reaction on Pd catalysts indicates the poisoning of intermediates.[46–48] However, the current decay for the reaction

Table 3. Physic surface area (*S*) and electrochemical active surface area (EASA) of Pd NPs, mass peak current density (I_p) and onset potential (E_p) of alcohols oxidation reaction on Pd-CNTs.

Sample	EASA	Methanol		Ethanol		Ethylene glycol	
	[m^2 g^{-1}]	I_p [mA mg^{-1}]	E_p [V]	I_p [mA mg^{-1}]	E_p [V]	I_p [mA mg^{-1}]	E_p [V]
Pd-CNTs-1	30.4	317	0.513	1484	0.400	1345	0.454
Pd-CNTs-2	36.2	818	0.457	2858	0.353	2095	0.409
Pd-CNTs-3	44.8	780	0.478	2469	0.383	1975	0.420
Pd-CNTs-4	26.2	501	0.490	1574	0.394	1534	0.450
Pd/C	–	236[42]	0.540[42]	360[43]	0.503[43]	1000[44]	0.608[44]

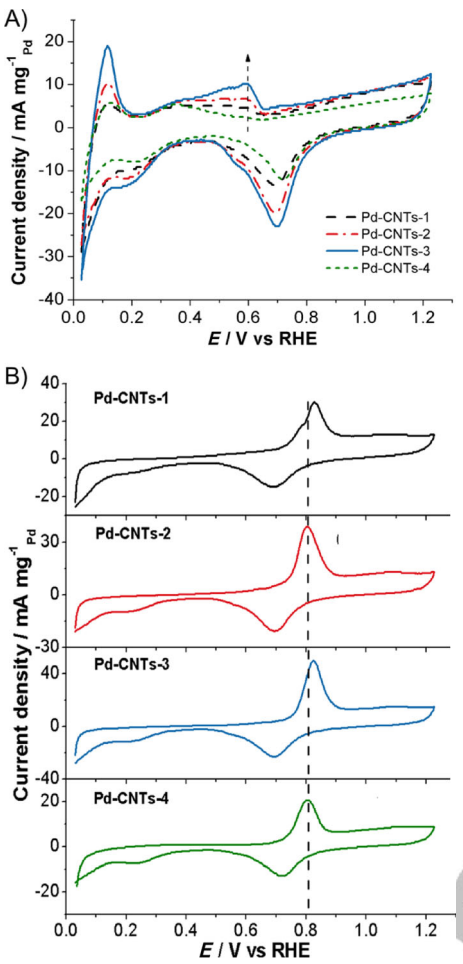

Figure 4. (A) Cyclic voltammetry of Pd-CNTs catalyst at N_2-saturated 1.0 M KOH and (B) CO stripping voltammograms of Pd-CNTs catalysts. Pd loading was 0.05 mg cm^{-2} and scan rate was 20 mV s^{-1} at 25 °C.

on Pd-CNTs-2 and Pd-CNTs-3 is significantly slower than that on Pd-CNTs-1 and Pd-CNTs-4 for the oxidation reaction of alcohols in alkaline solution. For instance, the current density of Pd-CNTs-2 and Pd-CNTs-3 for MOR at $t = 1000$ s is 86.5 mA mg^{-1} and 55.7 mg mg^{-1}, respectively, which is significantly higher than 10.5 mA mg^{-1} and 13.1 mA mg^{-1} for Pd-CNTs-1 and Pd-CNTs-4, respectively. The current density of Pd-CNTs measured at $t = 1000$ s against the wall numbers of CNTs also shows distinctive volcano curves for the ethanol and EG oxidation reaction (Figure 7D and F). This indicates that CNTs support with 3–7 walls significantly promotes the tolerance and resistance of Pd toward the poisoning effect of intermediate species of the alcohol oxidation reaction.

We also studied the charge-transfer property of Pd-CNTs for alcohols oxidation by electrochemical impedance spectroscopy (EIS). Figure 8 shows the Nyquist plots for the MOR on Pd-CNTs measured at 0.77 V. The obvious inductive loops in low frequencies indicates that the intermediate of MOR, CO_{ads}, decreased with the increase of the potential because of redundant OH_{ads} covered on the Pd surface.[49] Moreover, the equivalent circuit analysis (Inset in Figure 8) indicates that the charger-transfer resistance (R3) of Pd-CNTs-2 and Pd-CNTs-3 is 19.1 and 41.4 Ω cm^{-2}, substantially lower than 104.9 and 77.5 Ω cm^{-2} for the reaction on Pd-CNTs-1 and Pd-CNTs-4, respectively (Table S2, Supporting Information). The significantly low value of charge-transfer resistance implies the energy barrier for the reaction on Pd-CNTs-2 and Pd-CNTs-3 is much lower, as compared to that on Pd-CNTs-1 and Pd-CNTs-4, consistent with the polarization results.

Promotion mechanism of CNTs

Before the discussion on the promotion mechanism of CNTs, let us first to examine the possible effect of other factors such as impurities, surface oxygen-containing groups, surface area of CNTs and Pd NPs, and the interaction between Pd NPs and CNTs on the electrocatalytic activities of supported Pd NPs for the oxidation reaction of alcohols.

· Impurities: In order to eliminate the effect of metal impurities in CNTs for the alcohol oxidation, concentrated HCl solution was used to dissolve the metals. ICP-OES analysis indicated that the amounts of metallic impurities (e.g., Fe, Co, Ni and Mo) are sharply reduced to about 100 ppm in the CNTs. Carmo et al found out that the performance of the PtRu/CNTs catalyst was similar to that of the PtRu/C, although CNTs contained the same amount of metal impurities (Fe, Co, and Ni) as PtRu catalyst,[14] indicating that the metal contaminates of the CNTs do not contribute to the MOR of PtRu. This is consistent with the present study that the low level of metallic impurities in CNTs do not contribute to the alcohol oxidation reactions (see Figure 5).

· Oxygen containing groups: The oxygen-containing groups derived from the defect of CNTs-2 and CNTs-3 are higher than CNTs-1 and CNTs-4. However, the content of oxygen containing groups of CNTs-4 is 6.2%, close to 6.7% of CNTs-3, but the activity and stability of Pd-CNTs-4 is much lower than that of Pd-CNTs-3. The overlapped CV curves for pristine CNTs in 1.0 M KOH and 1.0 M KOH + 1.0 M ethanol solutions indicate that the oxygen-containing groups is unlikely to contribute to the oxidation reactions for Pd-CNTs directly. Moreover, Nakamura et al found that defect-free CNTs show a much higher CO tolerance than defective CNTs.[50] Raman results also indicate that the defect of CNTs increased with the wall number of CNTs. Thus, the content of oxygen-containing groups is unlikely the predominant factor to affect the activity of Pd-CNTs for alcohol oxidation reactions.

· PdO: It has been shown that Pd NPs expressed an electronic structure similar to Pt because of a thin layer of PdO.[51] PdO, like RuO_2, sufficiently pulls the methyl group off the α-carbon of the intermediate CH_3CO, and also donates oxygen-containing species (OH_{ads}) to promote the oxidation of CO to CO_2, facilitating the EOR on Pd catalyst.[52] Thus, high PdO content in Pd-CNTs may result in high alcohol-oxidation activity. As shown in Table 2, content of Pd^{II} of Pd-CNTs-4 is 67.3%, highest among the Pd NPs catalysts. However, the activity of Pd-CNTs-4 is close to that Pd-CNTs-1 and substantially lower than Pd-CNTs-2 and Pd-CNTs-3. Thus, similar to the oxygen-containing groups, PdO content does not play a critical role in the electrocatalytic activity of Pd NPs supported on CNTs.

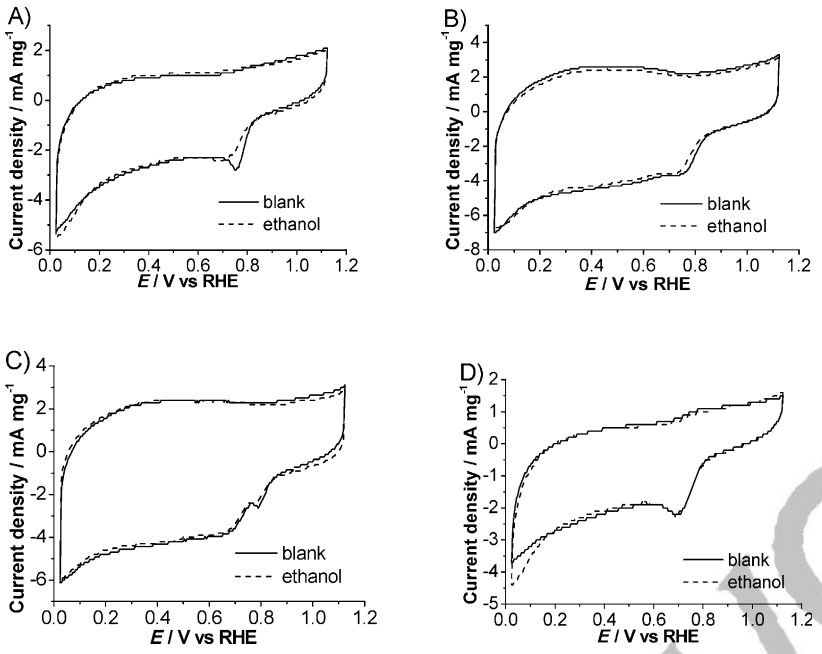

Figure 5. Cyclic voltammetry of (A) CNTs-1, (B) CNTs-2, (C) CNTs-3 and (D) CNTs-4, measured at 1 M KOH and iM KOH + 1 M ethanol solutions. Solid lines were the blank experiments measured in 1.0 M KOH solution, and the dotted lines were measured in 1.0 M ethanol + 1.0 M KOH solution. CNTs loading was 0.026 mg cm^{-2}, and scan rate was 100 mV s^{-1}.

· Surface area: MOR, EOR, and EGOR in alkaline systems have been extensively studied and it is accepted that alcohol-oxidation reaction on Pd NPs generally follows the surface catalytic procedures.[53,54] The CNTs-1 support has the highest surface area of 577 m^2 g^{-1} as compared to other CNTs, but the electrocatalytic activity of Pd-CNTs-1 is significantly lower than that of Pd-CNTs-2 and Pd-CNTs-3 (Figure 6 and 7). Based on the Pd NPs loading and assumed the spherical shape of Pd NPs, the surface areas of Pd NPs were calculated as 238, 200, 227, and 178 m^2 g^{-1} for Pd-CNTs-1, Pd-CNTs-2, Pd-CNTs-3, and Pd-CNTs-4, respectively. Clearly the surface area of Pd NPs does not follow particular relationship with the number of walls of CNTs. According to the CO-stripping test, Pd-CNTs-3 has EASA of 45 m^2 g^{-1}, ~24% higher than that of Pd-CNT-2. However, the mass activity Pd-CNTs-3 for EOR is 13.6% lower than that of Pd-CNTs-2. This indicates other factors affect the alcohols oxidation activities of Pd-CNTs in alkaline system besides EASA and surface areas.

· Interaction between CNTs and Pd NPs: The interaction or bonding between the Pd NPs and CNTs plays an important role in the electrocatalytic activity and stability of supported Pd-based NPs. For instance, the crystalline Pt NPs interacted with CNTs through synergic bonding involving charge redistribution between C2p-derived states and Pt5d bands due to the presence of unsaturation in the graphene sheets (delocalized π orbitals).[55] Such a bonding scheme would facilitate the uniform dispersion and immobilization of Pd NPs on the CNT surface, which would prevent lateral diffusion of Pd NPs under fuel cell operating conditions. This may be the reason for the high electrocatalytic activities of Pd NPs supported on CNTs, as compared to Pd NPs supported on high surface area carbon (see Table 3). However, in the case of Pd-CNTs, the binding energy of metal Pd^0 at $3d_{3/2}$ = 341.1 eV and $3d_{5/2}$ = 335.8 eV in Pd-CNTs are almost the same for the four Pd-CNTs, implying that the interaction of CNTs and Pd NPs could not be the reason for the significant differences in the electrocatalytic activity of Pd NPs supported on CNTs with different number of walls.

We have shown earlier that the electrocatalytic activity of pristine CNTs for the oxygen evolution reaction (OER) of water electrolysis in alkaline solutions shows a distinctive volcano-curve, ■■dependent ■■on the number of walls of CNTs. CNTs with 2–7 walls have excellent activity, fast kinetics and much lower energy barrier for OER in alkaline solutions, as compared with the SWNTs and MWNTs.[24] The results indicated that there may exist a dual functionality of CNTs with specific number of walls; the outer wall provides reaction sites for the absorption and dissociation of OH^-, OOH* species, while the intact inner-tube serves as the effective electronic conducting pathway for the charge-transfer process of the reaction via electron tunneling between the outer wall and inner tubes.

Most significantly, the mass activity of Pd-CNTs demonstrates the distinctive volcano-shape for methanol, ethanol, and ethylene glycol oxidation as a function of the wall number of CNTs (Figure 9), similar to the OER activity of pristine CNTs.[24] Vizuete et al.[56] attached dimethylanilino (DMA) to the external surface of DWNTs and SWNTs and observed the shorter transient signal for DMA/DWNTs than DMA/SWNTs via nanosecond laser flash photolysis. The fast electrons/DMA·$^+$ recombination rate of DMA/DWNTs was explained by the migration of the electrons and holes from the outer wall of DWNTs where the charge separation occurs on the inner walls of DWNTs. The tunneling effect between outer layer and the inner layer of unmodified DWNTs was also observed by Kalbac et al by using in situ Raman spectro-electrochemistry.[57] They addressed the finding that when the electronic states of the outer layer are filled with holes or electrons, and if those filled states are higher in energy than those of the inner layer, the charge will transfer from the outer tube to the inner tube. The first-principles calculations of DWNTs evidenced the hybridization of electronic wave functions of the outer and inner tubes, suggesting electron transportation between these two tubes.[58] Thus, the electron tunneling mechanism between the outer wall and inner tubes could also occur for the alcohol oxidation reactions on Pd-CNTs, similar to that observed for OER on CNTs.[24]

Figure 10 shows schematically the possible processes for the alcohol oxidation reactions on Pd-CNTs in alkaline solutions.

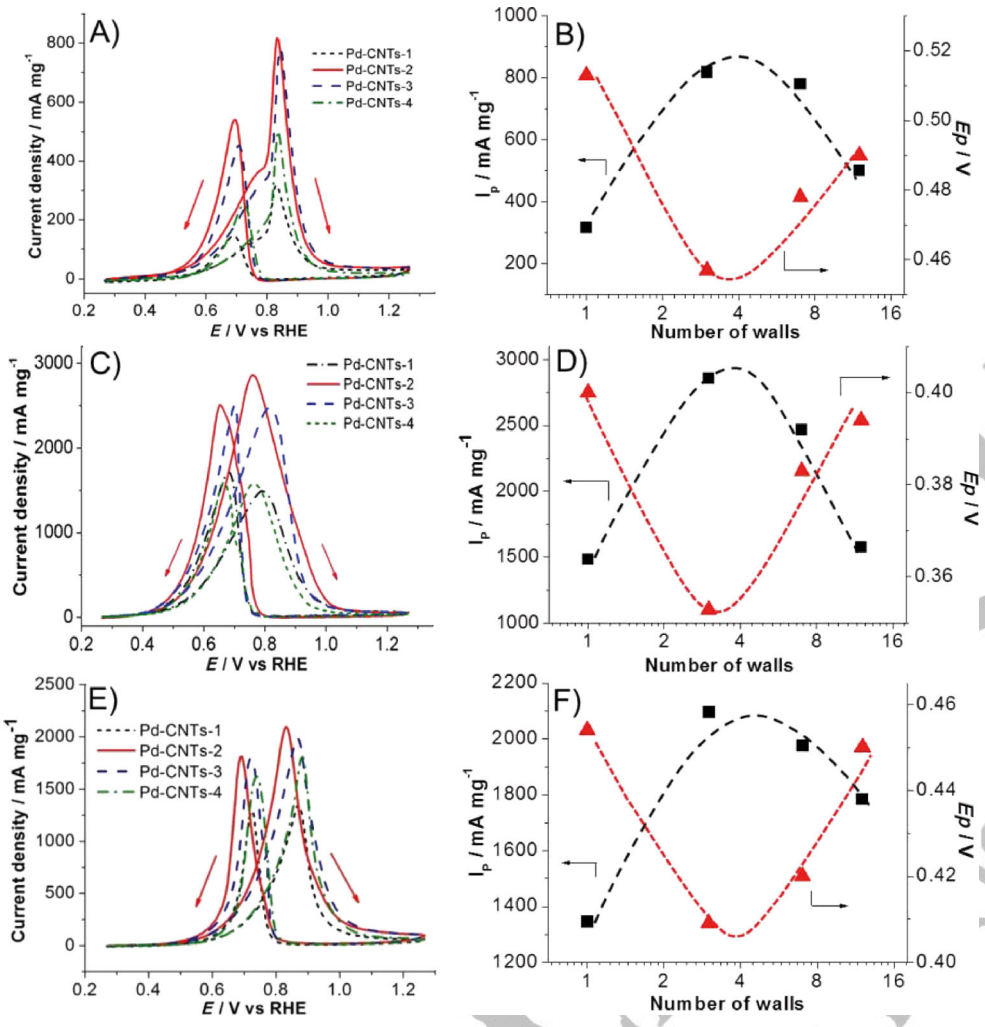

Figure 6. (A,C,E) Cyclic voltammetry profiles of Pd-CNTs catalysts for methanol, ethanol oxidation and ethylene glycol oxidation, respectively, at scan rate 50 mV s^{-1}. (B, D, F) The corresponding plots of the forward peak current density and onset potential of Pd-CNTs against the wall numbers of CNTs for the oxidation reaction of methanol, ethanol and ethylene glycol, respectively. The alcohols concentration was 1.0 M in 1 M KOH and Pd loading was 0.05 mg cm^{-2}.

The oxidation reaction of alcohols (R-CH_2OH) occurs on the catalytic sites of Pd NPs assembled on CNTs, forming various intermediates in addition to adsorbed CO (represented by R-CO/CO). In the case of EOR, the intermediates would involve CH_3CO and CO.[59] The electrooxidation of more complicated alcohols such as EG is a complex process as up to 10 electrons per molecules is required for full oxidation to CO_2. The reaction would proceed via several consecutive and/or parallel steps involving different reaction intermediates of C_2 (glycolate, glyoxal, glyoxylate, and oxalate) and C_1 species (formate and carbonate).[47,48,60] Thus the reaction rate of the electrocatalysts for alcohol oxidation reaction would strongly depend on the charge transfer and the effective oxidation/removal of the adsorbed intermediates. As shown by Liang et al.,[59] rate-determining step for EOR is the removal of the adsorbed ethoxy,■■OK?■■ CH_3CO_{ads}, and CO. In the case of Pd NPs supported on CNTs, the released electrons during the oxidation reaction, i.e., the formation of intermediates, R-CO/CO and the final products, CO_2 (or CO_3^{2-} due to the formation of carbonate in alkaline solution) and R-COO^- representing various C1 and/or C2 species, would transfer to the inner tubes of CNTs from the outer wall through the electron tunneling mechanism under the electrochemical polarization driving force, as discussed above. The intact inner-tube serves as the effective electronic conducting pathway for the charge-transfer process of the reaction. Such effective charge transfer would not be possible for the Pd NPs supported on SWNTs and for Pd-CNTs-1. ■■OK?■■Furthermore, the enhancement effect of the CNTs for the alcohol oxidation reactions diminishes as the number of walls increases when the wall number is higher than seven due to the significantly reduced polarization driving force or dc bias across the walls or layers of CNTs for the electron tunneling between the outer wall and inner tubes. Thus, the charge transfer for the alcohol oxidation reactions on Pd-CNTs-2 and Pd-CNTs-3 will be much faster via the electron tunneling mechanism between the outer wall and inner tubes as compared to that of Pd-CNTs-1 and Pd-CNTs-4, similar to that observed for OER on CNTs with 2–7 number of walls.[24]

The adsorption and migration or diffusion of active oxygen-containing species, OH_{ads}, on the outer wall surface of CNTs would also be facile, promoted by the fast charge transfer under the influence of the electron tunneling effect. The steady supply of active OH_{ads} species lead to the fast stripping and removal of adsorbed intermediates such as CO and/or R-CO species, forming CO_2/CO_3^{2-} and/or R-COO^- and releasing active sites on Pd NPs supported on CNTs with 3–7 concentric tubes or walls for alcohol oxidation reaction. That is most likely the reason why the alcohol oxidation activity of Pd-CNTs-2 and Pd-CNTs-3 is significantly higher than Pd-CNTs-1 and Pd-CNTs-4.

Conclusions

Pd NPs with controlled particle size have been uniformly assembled and anchored on the surface of CNTs with different graphitic layers. Pd NPs supported on CNTs with 3–7 walls, show a significantly higher activity and stability for the oxidation reaction of methanol, ethanol and ethylene glycol, as

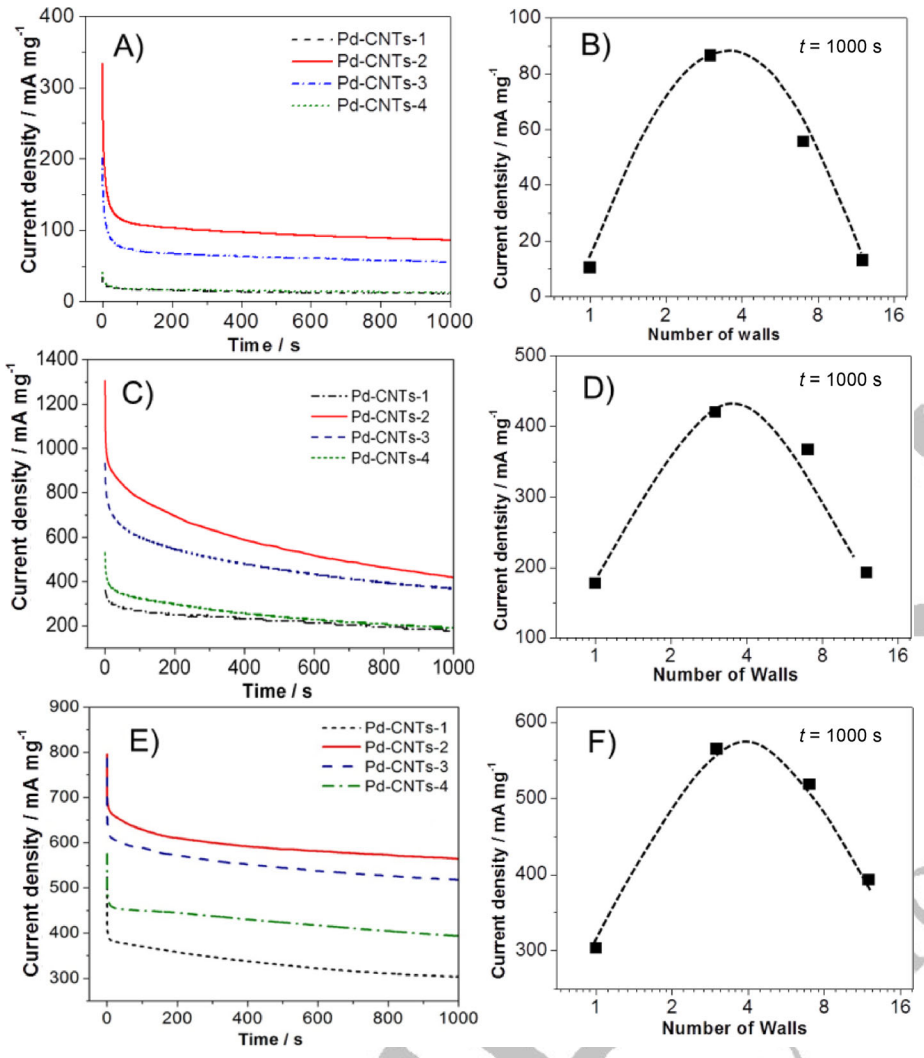

Figure 7. (A,C,E) Chronoamperometry curves of Pd-CNTs catalysts for the oxidation of methanol measured at 0.67 V vs RHE, ethanol measured at 0.67 V vs RHE and ethylene glycol measured at 0.77 V vs RHE, respectively. (B,D,F) Corresponding current density plots of Pd-CNTs measured at $t = 1000$ s for the oxidation of methanol, ethanol and ethylene glycol, respectively. The alcohols concentration was 1.0 M in 1 M KOH and Pd loading was 0.05 mg cm^{-2}.

compared to Pd NPs supported on SWNTs and MWNTs. ■■The names of the samples CNTs-1 etc. have been removed to improve clarity of Conclusion section ■■The results show that significantly high activity of Pd NPs supported on CNTs with 3–7 walls is not related to the traces of impurities in CNTs, EASA of Pd NPs or specific surface areas of CNTs, the oxygen groups on CNTs or the interaction between the Pd NPs and CNTs. The alcohol oxidation reaction on Pd NPs supported on CNTs with 3–7 walls is much faster and more stable, as compared to that on Pd NPs supported on conventional SWNTs and MWNTs due to the effective charge transfer steps and effective removal of intermediate species by active oxygen-containing species, OH_{ads} under the influence of the efficient electron-tunneling effect between the outer wall and inner tubes of CNTs.

In addition to the significant promotion effect of addition of Ni-Zn, Au, Sn, W, and oxides such as Co_3O_4, etc., to Pd-based electrocatalysts for alcohol oxidation reactions,[2,7,46,61] the present studies demonstrate clearly that the electrocatalytic activity of Pd NPs can also be significantly enhanced by manipulating the quantum properties and electron-tunneling effect of inner tubes of CNTs supports.

Experimental Section

Chemicals

Four different CNTs with number of walls from 1 to 16 were selected and were purchased from Nanostructrued & Amorphous Materials Inc.[20] These CNTs were fabricated by catalytic chemical vapor deposition method. The CNTs were ultrasounded by 32 wt% HCl (Ajax Finechem) for 6 h and then stirred at room temperature for 48 h before use. The procedures were repeated twice. Nafion suspension (5 wt%) was purchased from DuPont Inc. Other chemicals including $PdCl_2$, tetrahydrofuran (THF), ethanol, EG were purchased from Sigma–Aldrich, and were used as received without further purifications. MilliQ water was used in the experiments.

Pd-CNTs catalyst synthesis

CNTs were first functionalized by THF before the assembly of Pd NPs. The use of THF solvent rather than nitrogen-containing polyelectrolytes as non-covalent functionalization agent is to avoid the additional electrocatalytic effect of the functional groups of the polyelectrolytes on the properties of supported catalysts.[62] In this method, 10 mg of $PdCl_2$ and 0.25 mL of 32 wt% HCl were added to 3.0 mL of THF in 8.0 mL glass vial and were stirred at room temperature for several minutes until transparent brown solution was obtained. $PdCl_2$ in HCl solution would dissociate, forming the negatively charged $[PdCl_4]^{2-}$ in the solution. Moreover, THF molecules display positive charge after protonation in the acid solution. Thus, $[PdCl_4]^{2-}$ and THF molecules form $[PdCl_4]^{2-}$/THF pairs through the electrostatic force. Then, 24 mg purified CNTs were added to the solution and subsequently sonicated for approximately 15 min to achieve a homogenous dispersion. $[PdCl_4]^{2-}$/THF pairs are attached to the CNTs surface via π–σ stacking. Excess THF solvent was evaporated by continuous stirring of the dispersion at room temperature and the solids product was dried at 40 °C overnight. After grounding in an agate mortar, the resulting solids were then heated in a tube furnace at 150 °C under 100 SCCM of H_2 for 2 h to reduce $[PdCl_4]^{2-}$ to Pd NPs and to decompose and evaporate the THF functionalization molecules. Pd loading on Pd-CNTs-1, Pd-CNTs-2, Pd-CNTs-3, Pd-CNTs-4 was 20.0%, 27.1%, 20.1% and 25.2%, respectively, as determined by TGA (Figure S2, Supporting Information), and were collected and stored under a vacuum desiccator.

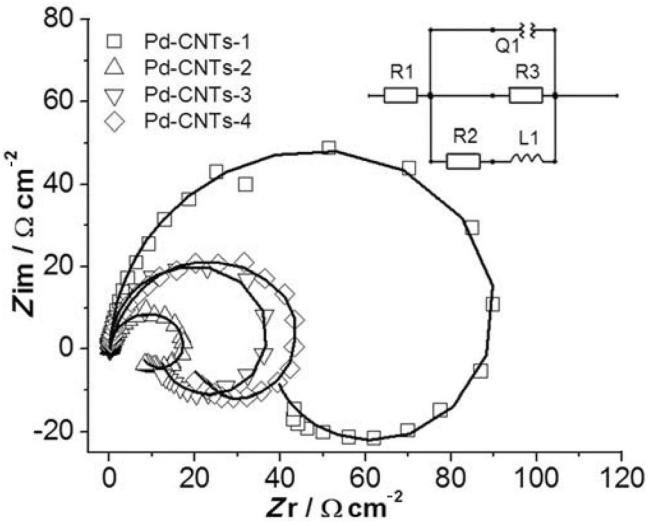

Figure 8. Nyquist plot of EIS of Pd-CNTs catalyst for methanol oxidation reaction, measured at 0.77 V in 1 M KOH + 1 M methanol. The symbols are the experimental data and the lines are the fitted curve based on the equivalent circuit of MOR on Pd-CNTs. In the equivalent circuit, R1 is the solution resistance, R2 is the inductive resistance, R3 is the charge transfer resistance, Q1 is the constant phase element, and L1 is the inductance. ■■ Please check units of axes. We changed them ohm cm^{-2} to match text. ■■

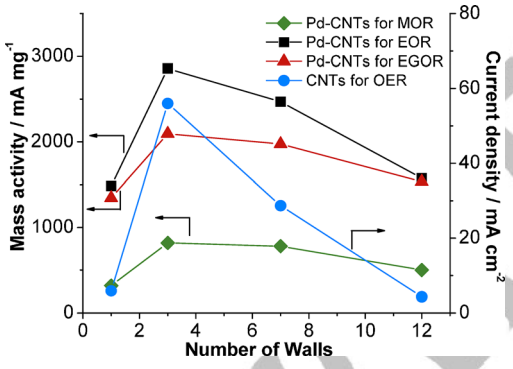

Figure 9. Mass specific activity of Pd-CNTs catalysts based on the forward current density for the oxidation reactions of methanol, ethanol and ethylene glycol in alkaline solutions. Pt loading was 0.05 mg cm^{-2}. The current density for oxygen evolution reaction (OER) were measured at 1.8 V vs RHE in 1 M KOH solution with scan rate of 1 mV s^{-1} and CNT loading of 0.025 mg cm^{-2}.[24]

Physical and electrochemical characterizations

The CNTs were characterized by the Raman spectroscopy with excited wavelength of 1640 cm^{-1} (0.21 eV) and power density of 5 mW cm^{-2}. Morphologies of CNTs and Pd-CNTs were examined by transmission electron microscopy (TEM, JEOL 3000F) with operation voltage of 200 kV. The BET surface area and porosity of CNTs were investigated by Micromeritics Tristar II. The samples were first degassed at 150 °C for 24 h and then analyzed at 77 K. X-ray photoelectron spectroscopy (XPS) measurements are conducted by using a ESCALAB 250 spectrometer with an $Mg_{K\alpha}$ radiator.

The electrocatalytic activity of as-synthesized Pd-CNTs catalyst was studied by cyclic voltammetry (CV) in 1.0 M KOH + 1.0 M methanol, 1.0 M KOH + 1.0 M ethanol and 1.0 M KOH + 1.0 M EG solutions. Catalyst electrodes were prepared by mixing the Pd-CNTs powder with 5.0 wt% Nafion solution. The mixture was sonicated at room

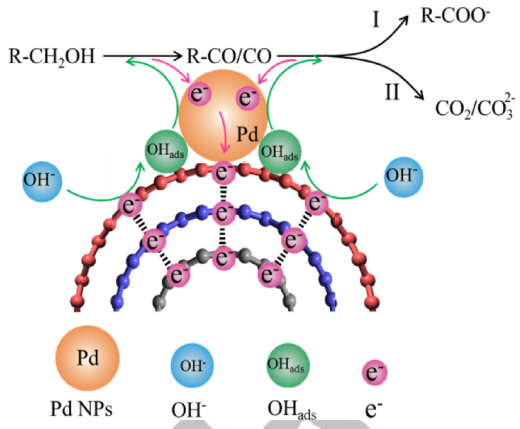

Figure 10. Scheme of alcohol oxidation reactions on Pd NPs supported on CNTs with 3–7 walls, promoted by the accelerated charge transfer process between the outer wall and inner tubes of CNTs *via* effective electron tunneling under electrochemical polarization driving force and by the fast stripping and removal of adsorbed intermediates such as CO and/or R-CO species facilitated by active OH_{ads} species, forming CO_2/CO_3^{2-} and/or $R\text{-}COO^-$ final products.

temperature for 2 h before 10 μL catalyst ink was applied onto a glassy carbon disk with a diameter of 7 mm. After solvent evaporation, a thin layer of catalyst with 0.05 mg cm^{-2} Pd loading was deposited on the glassy carbon electrode surface as the work electrode. A Pt plate and Hg/HgO (1.0 M KOH) (0.92 V vs RHE) electrode were used as the counter and reference electrodes, respectively. All electrochemical tests were carried out on IVIUMSTAT potentiostat (Ivium technology, Netherland). Blank cyclic voltammetry tests were conducted in 1.0 M KOH solution. The stability of Pd-CNTs catalysts for methanol, ethanol and EG oxidation reactions was evaluated, using chronoamperometry at 0.67 V in 1.0 M KOH + 1.0 M methanol and 1.0 M KOH + 1.0 M ethanol and at 0.77 V in 1.0 M KOH + 1.0 M EG solutions. The electrochemical impedance spectra (EIS) of Pd-CNTs for methanol were measured at 0.77 V in 1.0 M KOH + 1.0 M methanol from 100 kHz to 0.1 Hz.

CO stripping of Pd-CNTs was conducted in N_2 saturated 1.0 M KOH solution. After bubbling N_2 to 1.0 M KOH 30 min, CV was measured in the range of 0.02 V–1.22 V vs Hg/HgO (1.0 M KOH) at a scan rate of 20 mV s^{-1} for the blank test. The solution was saturated with CO and chronoamperometry was conducted at 0.12 V vs Hg/HgO (1.0 M KOH) for 30 min for adsorption monolayer of CO on Pd surface. Then N_2 was bubbled into the solution again to remove redundant CO in the solution, followed by CV measurement with the same condition as the blank test. Electrochemical active surface area (EASA) of Pd NPs was calculated according to equation $EASA = Q/Cm$, where Q associates with the Coulombic amount, while C is the reduction charge of PdO monolayer (405 μC cm^{-2}),[63] and m is the mass of Pd on the glassy carbon electrode surface.

Acknowledgements

This work is financially supported by the Australian Research Council (Project number: DP120104932 & DP150102044) and the Major International (Regional) Joint Research Project of NNSFC (5121002), China. The authors acknowledge the facilities, and the scientific and technical assistance of the National Imaging Facility at the Centre for Microscopy, Characterisation & Analysis, the

University of Western Australia, a facility funded by the University, State and Commonwealth Government.

Keywords: alcohol oxidations · carbon nanotubes · electron tunneling effect · Pd nanoparticles · volcano curves

[1] Y.-S. Ye, M.-Y. Cheng, X.-L. Xie, J. Rick, Y.-J. Huang, F.-C. Chang, B.-J. Hwang, *J. Power Sources* **2013**, *239*, 424 – 432.
[2] A. Marchionni, M. Bevilacqua, C. Bianchini, Y. X. Chen, J. Filippi, P. Fornasiero, A. Lavacchi, H. Miller, L. Q. Wang, F. Vizza, *ChemSusChem* **2013**, *6*, 518 – 528.
[3] C. W. Xu, H. Wang, P. K. Shen, S. P. Jiang, *Adv. Mater.* **2007**, *19*, 4256 – 4259.
[4] C. Xu, L. Cheng, P. Shen, Y. Liu, *Electrochem. Commun.* **2007**, *9*, 997 – 1001.
[5] F. P. Hu, Z. Wang, Y. Li, C. Li, X. Zhang, P. K. Shen, *J. Power Sources* **2008**, *177*, 61 – 66.
[6] G. Hu, F. Nitze, H. R. Barzegar, T. Sharifi, A. Mikolajczuk, C.-W. Tai, A. Borodzinski, T. Wagberg, *J. Power Sources* **2012**, *209*, 236 – 242.
[7] S. M. Alia, K. Duong, T. Liu, K. Jensen, Y. S. Yan, *ChemSusChem* **2014**, *7*, 1739 – 1744.
[8] V. Bambagioni, C. Bianchini, A. Marchionni, J. Filippi, F. Vizza, J. Teddy, P. Serp, M. Zhiani, *J. Power Sources* **2009**, *190*, 241 – 251.
[9] Y. B. Yan, Y. T. Chen, X. L. Jia, Y. H. Yang, *Appl. Catal. B* **2014**, *156*, 385 – 397.
[10] H. Huang, X. Wang, *J. Mater. Chem. A* **2014**, *2*, 6266 – 6291.
[11] H. T. Zheng, Y. Li, S. Chen, P. K. Shen, *J. Power Sources* **2006**, *163*, 371 – 375.
[12] R. N. Singh, R. Awasthi, *Catal. Sci. Technol.* **2011**, *1*, 778 – 783.
[13] E. Antolini, *Appl. Catal. B* **2009**, *88*, 1 – 24.
[14] M. Carmo, V. A. Paganin, J. M. Rosolen, E. R. Gonzalez, *J. Power Sources* **2005**, *142*, 169 – 176.
[15] G. Wu, B.-Q. Xu, *J. Power Sources* **2007**, *174*, 148 – 158.
[16] P. Trogadas, T. F. Fuller, P. Strasser, *Carbon* **2014**, *75*, 5 – 42.
[17] E. S. Steigerwalt, G. A. Deluga, C. M. Lukehart, *J. Phys. Chem. B* **2002**, *106*, 760 – 766.
[18] J. Li, A. Cassell, L. Delzeit, J. Han, M. Meyyappan, *J. Phys. Chem. B* **2002**, *106*, 9299 – 9305.
[19] W. Li, X. Wang, Z. Chen, M. Waje, Y. Yan, *J. Phys. Chem. B* **2006**, *110*, 15353 – 15358.
[20] J. Zhang, Y. Cheng, S. F. Lu, L. C. Jia, P. K. Shen, S. P. Jiang, *Chem. Commun.* **2014**, *50*, 13732 – 13734.
[21] T. Kim, G. Kim, W. I. Choi, Y.-K. Kwon, J.-M. Zuo, *Appl. Phys. Lett.* **2010**, *96*, ■■page numbers?■■.
[22] S. Osswald, E. Flahaut, Y. Gogotsi, *Chem. Mater.* **2006**, *18*, 1525 – 1533.
[23] I. D. Rosca, F. Watari, M. Uo, T. Akasaka, *Carbon* **2005**, *43*, 3124 – 3131.
[24] Y. Cheng, C. W. Xu, L. C. Jia, J. D. Gale, L. L. Zhang, C. Liu, P. K. Shen, S. P. Jiang, *Appl. Catal. B* **2015**, *163*, 96 – 104.
[25] V. M. Irurzun, M. P. Ruiz, D. E. Resasco, *Carbon* **2010**, *48*, 2873 – 2881.
[26] R. Graupner, *J. Raman Spectrosc.* **2007**, *38*, 673 – 683.
[27] A. M. Rao, S. Bandow, E. Richter, P. C. Eklund, *Thin Solid Films* **1998**, *331*, 141 – 147.
[28] S. Costa, E. Borowiak-Palen, M. Kruszynska, A. Bachmatiuk, R. J. Kalenczuk, *Mater. Sci. Poland* **2008**, *26*, 433 – 441.
[29] Z. J. Li, Z. W. Pan, S. Dai, *J. Colloid Interface Sci.* **2004**, *277*, 35 – 42.
[30] A. Peigney, C. Laurent, E. Flahaut, R. R. Bacsa, A. Rousset, *Carbon* **2001**, *39*, 507 – 514.
[31] O. Winjobi, Z. Zhang, C. Liang, W. Li, *Electrochim. Acta* **2010**, *55*, 4217 – 4221.
[32] W. Li, C. Liang, W. Zhou, J. Qiu, X. Zhou, G. Sun, Q. Xin, *J. Phys. Chem. B* **2003**, *107*, 6292 – 6299.
[33] R. D. Morgan, A. Salehi-khojin, R. I. Masel, *J. Phys. Chem. C* **2011**, *115*, 19413 – 19418.
[34] A. R. Siamaki, Y. Lin, K. Woodberry, J. W. Connell, B. F. Gupton, *J. Mater. Chem. A* **2013**, *1*, 12909 – 12918.
[35] W. Sun, Z. Liu, C. Jiang, Y. Xue, W. Chu, X. Zhao, *Catal. Today* **2013**, *212*, 206 – 214.
[36] V. Datsyuk, M. Kalyva, K. Papagelis, J. Parthenios, D. Tasis, A. Siokou, I. Kallitsis, C. Galiotis, *Carbon* **2008**, *46*, 833 – 840.
[37] R. Pattabiraman, *Appl. Catal. A* **1997**, *153*, 9 – 20.
[38] M. Simões, S. Baranton, C. Coutanceau, *Appl. Catal. B* **2010**, *93*, 354 – 362.
[39] M. C. Jeong, C. H. Pyun, I. H. Yeo, *J. Electrochem. Soc.* **1993**, *140*, 1986 – 1989.
[40] M. Noroozifar, M. Khorasani-Motlagh, M. S. Ekrami-Kakhki, R. Khaleghian-Moghadam, *J. Appl. Electrochem.* **2014**, *44*, 233 – 243.
[41] T. Ramulifho, K. I. Ozoemena, R. M. Modibedi, C. J. Jafta, M. K. Mathe, *J. Electroanal. Chem.* **2013**, *692*, 26 – 30.
[42] Y. Zhao, S. Nie, H. Wang, J. Tian, Z. Ning, X. Li, *J. Power Sources* **2012**, *218*, 320 – 330.
[43] H. Yan, Z. Bai, S. Chao, L. Yang, Q. Cui, K. Wang, L. Niu, *RSC Adv.* **2013**, *3*, 20332 – 20337.
[44] O. O. Fashedemi, K. I. Ozoemena, *Electrochim. Acta* **2014**, *128*, 279 – 286.
[45] S. Y. Wang, S. P. Jiang, T. J. White, J. Guo, X. Wang, *J. Phys. Chem. C* **2009**, *113*, 18935 – 18945.
[46] C. W. Xu, Z. Q. Tian, P. K. Shen, S. P. Jiang, *Electrochim. Acta* **2008**, *53*, 2610 – 2618.
[47] V. Bambagioni, M. Bevilacqua, C. Bianchini, J. Filippi, A. Marchionni, F. Vizza, L. Q. Wang, P. K. Shen, *Fuel Cells* **2010**, *10*, 582 – 590.
[48] J. L. Lin, J. Ren, N. Tian, Z. Y. Zhou, S. G. Sun, *J. Electroanal. Chem.* **2013**, *688*, 165 – 171.
[49] G. Wu, L. Li, B.-Q. Xu, *Electrochim. Acta* **2004**, *50*, 1 – 10.
[50] E. Yoo, T. Okada, T. Kizuka, J. Nakamura, *Electrochemistry* **2007**, *75*, 146 – 148.
[51] W. Ding, M. R. Xia, Z. D. Wei, S. G. Chen, J. S. Hu, L. J. Wan, X. Q. Qi, X. H. Hu, L. Li, *Chem. Commun.* **2014**, *50*, 6660 – 6663.
[52] K. Ding, Y. Wang, H. Yang, C. Zheng, Y. Cao, H. Wei, Y. Wang, Z. Guo, *Electrochim. Acta* **2013**, *100*, 147 – 156.
[53] H. An, L. Pan, H. Cui, B. Li, D. Zhou, J. Zhai, Q. Li, *Electrochim. Acta* **2013**, *102*, 79 – 87.
[54] Z. Y. Li, Y. J. Liang, S. P. Jiang, X. D. Shan, M. L. Lin, C. W. Xu, *Fuel Cells* **2012**, *12*, 677 – 682.
[55] J. G. Zhou, X. T. Zhou, X. H. Sun, R. Y. Li, M. Murphy, Z. F. Ding, X. L. Sun, T. K. Sham, *Chem. Phys. Lett.* **2007**, *437*, 229 – 232.
[56] M. Vizuete, M. J. Gómez-Escalonilla, S. García-Rodriguez, J. L. G. Fierro, P. Atienzar, H. García, F. Langa, *Chem. Eur. J.* **2012**, *18*, 16922 – 16930.
[57] M. Kalbac, A. A. Green, M. C. Hersam, L. Kavan, *Chem. Eur. J.* **2011**, *17*, 9806 – 9815.
[58] A. Lopez-Bezanilla, *J. Phys. Chem. C* **2013**, *117*, 15266 – 15271.
[59] Z. X. Liang, T. S. Zhao, J. B. Xu, L. D. Zhu, *Electrochim. Acta* **2009**, *54*, 2203 – 2208.
[60] R. B. de Lima, V. Paganin, T. Iwasita, W. Vielstich, *Electrochim. Acta* **2003**, *49*, 85 – 91.
[61] C. W. Xu, P. K. Shen, *Chem. Commun.* **2004**, 2238 – 2239.
[62] Y. Cheng, C. W. Xu, P. K. Shen, S. P. Jiang, *Appl. Catal. B* **2014**, *158*, 140 – 149.
[63] S. T. Nguyen, H. M. Law, H. T. Nguyen, N. Kristian, S. Wang, S. H. Chan, X. Wang, *Appl. Catal. B* **2009**, *91*, 507 – 515.

Received: January 20, 2015
Revised: March 1, 2015
Published online on ■■ ■■, 0000

These are not the final page numbers! ↗↗

*J. Zhang, S. Lu, Y. Xiang, P. K. Shen, J. Liu, S. P. Jiang**

■■ – ■■

Carbon-Nanotubes-Supported Pd Nanoparticles for Alcohol Oxidations in Fuel Cells: Effect of Number of Nanotube Walls on Activity

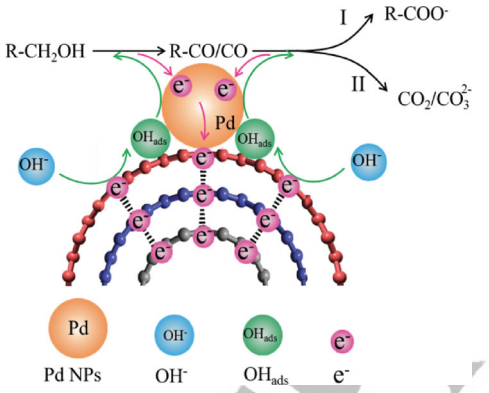

Three's the magic number: Palladium nanoparticles (NPs) with controlled particle size are uniformly assembled and anchored on the surface of carbon nanotubes CNTs with varying numbers of walls. Pd NPs supported on triple-walled CNTs (TWNTs) have the highest mass activity and stability for methanol, ethanol and ethylene glycol oxidation reactions, as compared to Pd NPs supported on single-walled and multi-walled CNTs.■■OK?■■

Pd nanoparticles on carbon nanotubes for alcohol oxidation in fuel cells @CurtinUni. SPACE RESERVED FOR IMAGE AND LINK

Share your work on social media! *ChemSusChem* has added Twitter as a means to promote your article. Twitter is an online microblogging service that enables its users to send and read text-based messages of up to 140 characters, known as "tweets". Please check the pre-written tweet in the galley proofs for accuracy. Should you or your institute have a Twitter account, please let us know the appropriate username (i.e., @accountname), and we will do our best to include this information in the tweet. This tweet will be posted to the journal's Twitter account @ChemSusChem (follow us!) upon online publication of your article, and we recommended you to repost ("retweet") it to alert other researchers about your publication.